Ultraviolet photochemistry and photophysics of weakly-bound (HI)2 clusters via high-n Rydberg time-of-flight spectroscopy

J. Zhang, M. Dulligan, J. Segall, Y. Wen, and C. Wittig

J. Phys. Chem., **1995**, 99 (37), 13680-13690• DOI: 10.1021/j100037a016 • Publication Date (Web): 01 May 2002

Ultraviolet Photochemistry and Photophysics of Weakly-Bound $(HI)_2$ Clusters via High-n Rydberg Time-of-Flight Spectroscopy

J. Zhang, M. Dulligan, J. Segall,† Y. Wen,‡ and C. Wittig*

Department of Chemistry, University of Southern California, Los Angeles, California 90089-0482

Received: March 3, 1995; In Final Form: May 25, 1995[⊗]

The high-n Rydberg time-of-flight (HRTOF) technique has been used to obtain translational energy distributions of hydrogen atoms deriving from weakly-bound $(HI)_2$ clusters photoexcited at 266 nm. A number of distinct features were observed and were used to establish much of the photophysics and photochemistry. Though the geometric structure of $(HI)_2$ has not been determined experimentally, equilibrium geometries have been estimated by using several semiempirical theoretical methods, all of which predict an approximately 90° L-shaped structure with one hydrogen localized between the two iodine atoms (the interior hydrogen) and the other pointing outward (the exterior hydrogen). Zero-point amplitudes are expected to be large. The photolytic removal of the exterior hydrogen yields I−HI and I*−HI radical−molecule clusters whose properties can be described, at least qualitatively, by using the formalism put forth by Hutson and co-workers, who carried out detailed calculations for the analogous Cl + HCl system. Photodissociation of the HI moiety whose hydrogen is *interior* can also yield radical−molecule clusters, as well as initiate intracluster reactive and/or inelastic scattering processes. Photoproducts that contain the HI chromophore such as $HI(v,j)$, I−HI, and I*−HI can also be efficiently photoexcited, yielding hydrogen atoms having signatures that reflect their parentages. Peaks in the translational energy distribution corresponding to photodissociation of HI in $v = 1$ and 2 are identified and confirmed by H → D substitution. Furthermore, $v = 0$ rotational levels having $7 \leq j \leq 13$ are just barely resolved. The most likely source of internally excited HI is believed to be inelastic scattering in which the internal hydrogen strikes the adjacent HI. This is deduced from the theoretical work of Aker and Valentini, who employed the method of quasiclassical trajectories with a potential surface developed by Last and Baer and modified by Clary. These calculations suggest that the likely L-shaped geometry of $(HI)_2$ is compatible with inelastic scattering via a failed reaction mechanism, whereas the hydrogen exchange reaction has low probability since it favors near-linear H−IH approaches. Low-energy shoulders offset slightly from the monomer peaks are most likely due to inelastic and elastic scattering of the internal hydrogen as it leaves. The photolysis of I*−HI clusters can be identified by an inelastic process in which I* is deactivated, thereby yielding hydrogen atoms having translational energies in excess of the highest monomer peak by slightly less than the iodine spin−orbit splitting. Such a peak in the TOF spectrum is observed. It is inevitable that some I_2 is formed with large interatom separation via the photolytic removal of hydrogen, which can occur by either H_2 formation (hydrogen abstraction) or sequential photolysis.

I. Introduction

The geometrical properties, intramolecular dynamics, photophysics, and photochemistry of weakly-bound clusters continue to provide conceptual, computational, and experimental challenges. Of the many weakly-bound systems presently available, the hydrogen halide pairs HX−HY have received particular attention because of the opportunities they offer for elucidating a number of interactions and mechanisms. To date, attention has been focused mainly on geometrical properties[1] and vibrational predissociation dynamics,[2] though studies of photoinitiated processes at ultraviolet wavelengths have been reported recently, both theoretically[3] and experimentally.[4−6] It is noteworthy that these systems are accessible to several complementary experimental techniques. Additionally, photo-induced processes of surface-bound hydrogen halide molecules[7] have also contributed to our understanding of the photochemistry of weakly-bound systems.

This paper reports results obtained with $(HI)_2$ clusters under molecular beam conditions that are strongly biased in favor of the formation of binary clusters over higher-than-binary clusters. A preliminary account has been given previously.[4] Pulsed laser photolysis at 266 nm is used to dissociate HI moieties, thereby initiating intracluster reactions, and elastic and inelastic scattering as well as forming weakly-bound radical−molecule clusters. Additionally, high laser fluences are used to effect the efficient sequential removal of both hydrogen atoms, opening the door to several intriguing interactions.

The 266 nm photodissociation of free HI yields iodine atoms in both the $^2P_{1/2}$(upper) and $^2P_{3/2}$(lower) states:

$$HI + h\nu \rightarrow I(^2P_{3/2}) + H \qquad E_{c.m.} = 12\,961\ cm^{-1} \quad (1)$$

$$\rightarrow I(^2P_{1/2}) + H \qquad E_{c.m.} = 5358\ cm^{-1} \quad (2)$$

where $E_{c.m.}$ is the product translational energy in the HI center-of-mass (c.m.) system for HI in its lowest quantum state. The $^2P_{1/2}$ quantum yield at 266 nm has been reported to be 0.35 ± 0.05 by Wilson and co-workers[8] and 0.40 ± 0.05 by Welge and co-workers,[9] and the 7603 cm^{-1} spin−orbit splitting results in the hydrogen atoms having two quite different speeds, i.e., 1.75 and 1.13 × 10^6 cm s^{-1} in the HI c.m. system. Moreover, the electronic transitions that yield the iodine spin−orbit levels are highly polarized, with $^2P_{3/2}$ deriving almost exclusively from

* To whom correspondence should be addressed.
† Present address: Metro Laser, 18006 Skypark Circle, Suite 108, Irvine, CA 92714.
‡ Present address: Department of Chemistry, University of Wisconsin, Madison, WI 53706.
⊗ Abstract published in *Advance ACS Abstracts,* August 15, 1995.

0022-3654/95/2099-13680$09.00/0

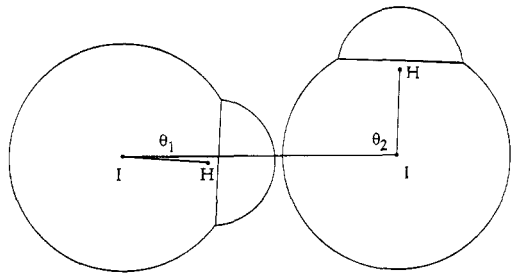

planar equilibrium

Figure 1. Theoretical estimate of the $(HI)_2$ planar equilibrium angles, taken from Buckingham and Fowler.[13] An iodine−iodine distance of ~5 Å is assumed from the work of Hannachi and Silvi.[14]

a perpendicular transition, while $^2P_{1/2}$ derives mainly from a parallel transition. The photodissociation of HX molecules has also been examined theoretically by Balint-Kurti,[10] Alexander,[11] and Shapiro,[12] who have derived $[^2P_{1/2}]/[^2P_{3/2}]$ population ratios. Detailed calculations were carried out for HCl/DCl[10,11] and HI/DI.[12]

In $(HI)_2$ clusters, the ultraviolet photodissociation of the HI moiety is expected to proceed in an analogous manner, at least when only the first of the HI moieties is photodissociated. However, the unique microcosm afforded by the weakly-bound cluster provides opportunities to study additional physical and chemical processes that go well beyond simple photodissociation.

The geometrical properties of $(HI)_2$ have not been measured. Though high-resolution spectroscopy is needed for secure geometrical definition, theoretical estimates provide a reasonable first guess.[13,14] Thus, the schematic drawing presented in Figure 1 of the theoretically-determined equilibrium geometry is intended to provide qualitative guidance. Though HI is a very weak Lewis acid, the fact that it is a good base (i.e., better than HF, HCl, and HBr)[13] leads us to believe that the equilibrium geometry is L-shaped. However, quantitative estimates of the angles, I−I distance, and zero-point amplitudes are left for the experts. The large zero-point excursions characteristic of such systems enable much more of the potential energy surface (PES) to be explored than just the equilibrium region. Estimates have also been made on the basis of matrix isolation studies,[15] but such data do not address the issue of structure directly. Nonetheless, these estimates also support an L-shaped geometry.

In photodissociation processes involving $(HI)_2$ clusters, the axes of the dissociating HI molecules are distributed according to the zero-point amplitudes for the intermolecular degrees of freedom. Consequently, the intact HI moiety sees atomic iodine electronic orbitals which are distributed as per the square of the intermolecular wave function. Thus, the triatom is expected to be formed with some vibronic excitation.

A methodology for constructing PES's of weakly-bound clusters containing open-shell atoms has been developed by Hutson and co-workers,[16] who have paid special attention to halogen atoms, examining the case of Cl−HCl in detail.[17] Spin−orbit interaction is accounted for explicitly, and their results, at least conceptually, can be applied to the present case. The beauty of their approach is that the Hamiltonian consists of parts that can be obtained with good accuracy from previous studies and/or separate theoretical estimates. Moreover, the role of spin−orbit interaction, while approximate, is transparent. The X−HX Hamiltonian is expressed as[16]

$$-\frac{\hbar^2}{2\mu R}\frac{\partial^2}{\partial R^2}R + \frac{\hbar^2}{2\mu R^2}\mathbf{L}^2 + H_X + H_{HX} + V_{inter} \qquad (3)$$

where R is the distance from the X atom to the HX c.m., $\mathbf{L}^2$ is an angular momentum operator for overall rotation, H_X is the X atom spin−orbit operator ($\xi\mathbf{l}\cdot\mathbf{s}$), H_{HX} is the HX rotation−vibration operator given by $B\mathbf{J}^2 + h\omega(\mathbf{a}^-\mathbf{a}^+ + {}^1/_2)$, and V_{inter} is a sum of terms:

$$V_{inter} = V_{Rg-HX} + V_{Rg-X} - V_{Rg-Rg} + V_{MP} \qquad (4)$$

where Rg stands for the nearest rare gas atom and V_{MP} is the attractive multipolar interaction involving the quadrupole of the halogen atom and the dipole and quadrupole of the hydrogen halide. It is straightforward to construct potential surfaces for the triatom systems in both diabatic and adiabatic representations. Because of its connection to the present study (despite the significant differences between chlorine and iodine), the theoretical results of Dubernet and Hutson for the Cl−HCl system[17] are reproduced in Figure 2. The diabats (left-hand column) are the diagonal elements of the Hamiltonian matrix calculated by using a coupled basis, characterized by the total (spin plus orbital) electronic angular momentum, j_a, and its polarization on the intermolecular axis, ω. The adiabats (right-hand column) are the eigenvalues. It should be noted that the $j_a = {}^1/_2$ surface is metastable in the sense that it can undergo radiationless transitions to one or both of the lower surfaces. The energy of the $j_a = {}^1/_2$ surface is presented relative to the energy of the atomic chlorine $^2P_{1/2}$ spin−orbit level.

The direct photodissociation of one of the HI moieties in $(HI)_2$ produces triatoms on a short time scale, and they commence life on PES's that are expected to bear qualitative similarity to those shown in Figure 2. Because of the extreme mass combinations, this occurs with minimal fragmentation; i.e., the hydrogen atom carries away nearly all the energy. The metastable $j_a = {}^1/_2$ species will eventually undergo fragmentation leading to ground state atomic iodine. However, this takes place over a much longer time scale than that of photolytic hydrogen removal, which occurs in <100 fs, even though our long duration pulses yield spatially extended wave packets. At high fluences, it is possible to photoexcite these metastable triatom clusters, as discussed below.

Weakly-bound I−HI and I−DI clusters have been observed in cryogenic matrices by using infrared spectroscopy.[15] Furthermore, their spectra in the range 250−450 nm have been characterized, albeit at a primitive level, and charge transfer states of I−HI resulting in spectral features at 325 and 387 nm have been reported.[15]

Some of the first hydrogen atoms that derive from the photodissociation of the HI moiety which contains the interior hydrogen can undergo intracluster collisions. In principle, both inelastic energy transfer and exchange reaction can occur. The hydrogen abstraction reaction yielding $H_2 + I_2$ is also possible, but our experiments are blind to this channel. Since it is also believed to be minor, it will not be discussed in detail.

Gerber and co-workers have used trajectory methods to examine photoinduced reactions in the analogous $(HCl)_2$ system, and both reactive and nonreactive collisions between H atoms and HCl molecules were identified and propensities were predicted.[3] In the case of $(HI)_2$, we will draw heavily from the comprehensive study of Aker and Valentini on H + HI interactions, i.e., experiments carried out under gas-phase, single-

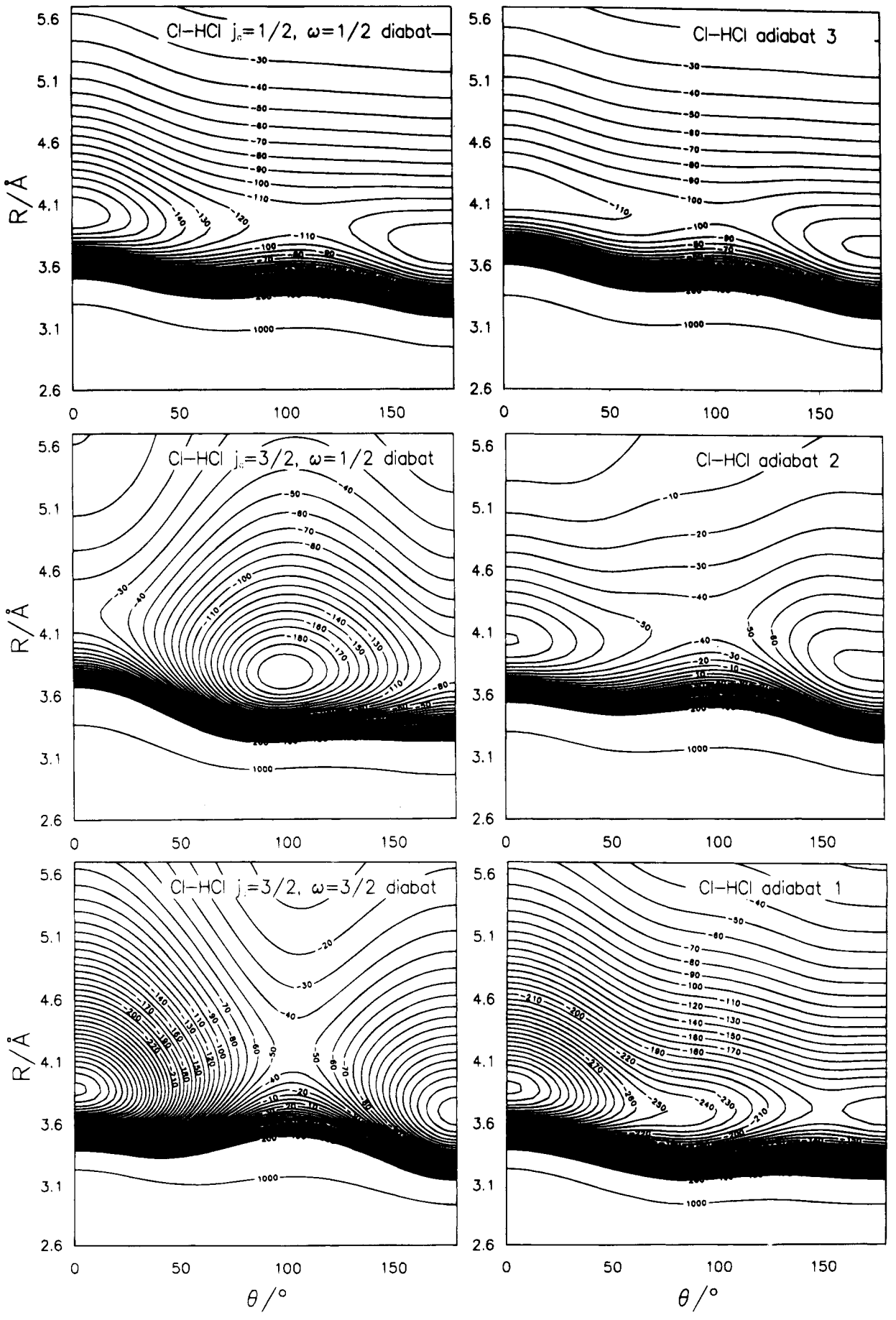

Figure 2. Calculated potential energy surfaces for the Cl + HCl system, taken from Dubernet and Hutson.[17] The left and right columns show diabats and adiabats, respectively.

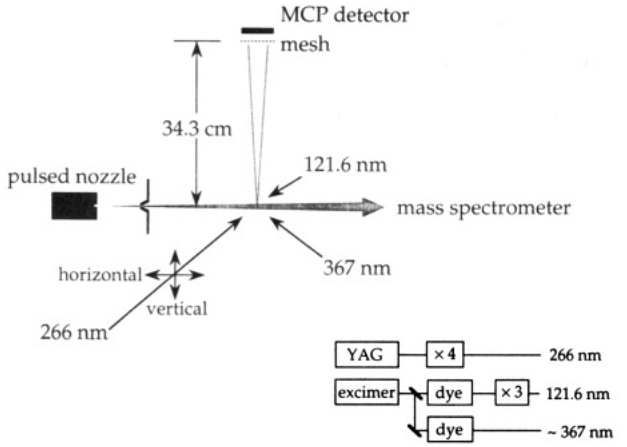

Figure 3. Schematic drawing of the experimental arrangement.

collision conditions[18] and theoretical estimates made by using the method of quasiclassical trajectories.[19]

In the material that follows, the experimental arrangement will be described briefly, since a full description has been given elsewhere.[20] Experimental results will then be presented followed by a discussion of the *a priori* possible physical and chemical interactions. The data will then be scrutinized within the context of these possible interactions. It will be shown that most of the experimental findings reported herein can be reconciled, at least qualitatively, with the theoretical predictions of Aker and Valentini,[19] who used a potential surface developed by Last and Baer[21] and refined by Clary.[22] Specifically, of the one-photon processes that yield $HI(v,j)$, it appears that the confined environment of the weakly-bound cluster favors inelastic scattering relative to the exchange reaction.

II. Experimental Arrangement

High-n Rydberg time-of-flight (HRTOF) spectroscopy[23] was employed (Figure 3). A pulsed molecular beam was produced by expanding 4−5% HI in He or Ar at total pressures of 700−3000 Torr. Mixtures were expanded into the source chamber through a 0.75 mm diameter pulsed nozzle operating at 10 Hz with a 500 μs pulse width. The molecular beam was differentially pumped and collimated by a 1 mm diameter skimmer located 2 cm downstream from the nozzle. The molecular beam was crossed with the 266 nm photolysis radiation 5 cm further downstream. The photolysis radiation was focused with a 70 cm focal length quartz lens; typically 1−25 mJ entered the vacuum chamber. The polarization purity of this radiation was better than 95%.

Nascent hydrogen atoms were excited by VUV radiation tuned to line center of the Lyman-α transition at 121.6 nm. This radiation was generated by tripling in Kr the 364.7 nm output from an excimer pumped dye laser, and it was focused into the interaction region with a MgF_2 lens. Another excimer pumped dye laser excited the H atoms from the 2^2P level to a high-n Rydberg level ($n = 40-90$). A weak dc electric field present in the laser interaction region breaks the isotropy of space and yields Rydberg atoms having large angular momentum quantum numbers. The high-n Rydberg states thus produced are radiatively metastable and stay highly excited for at least 10^{-4} s while they drift with their nascent velocities to the chevron microchannel plate detector. Upon arrival at the detector, the excited atoms are efficiently field-ionized as they pass a wire mesh; they are then detected as ions. TOF spectra were recorded by using a transient digitizer and were averaged and stored on a computer. The flight length was 34.3 cm. The sampling interval of the transient digitizer was 20 ns, and typically 1000−2000 channels around the region of interest were recorded; spectra represent between 3000 and 15 000 laser firings.

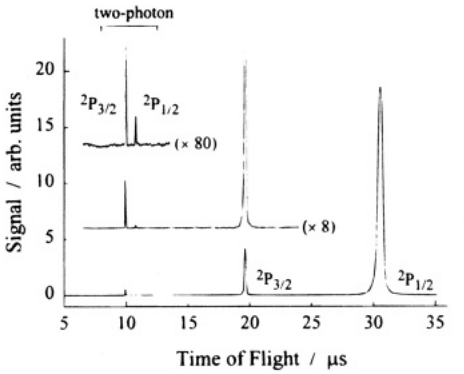

Figure 4. TOF spectrum of HI taken with vertical polarization (see Figure 3) and with essentially no clustering (4.4% HI/He, 760 Torr, early portion of the pulsed beam). A small amount of two-photon excitation yields very fast hydrogen atoms. Scale expansions show that the S/N is very good; even the smaller of the two-photon peaks is seen clearly.

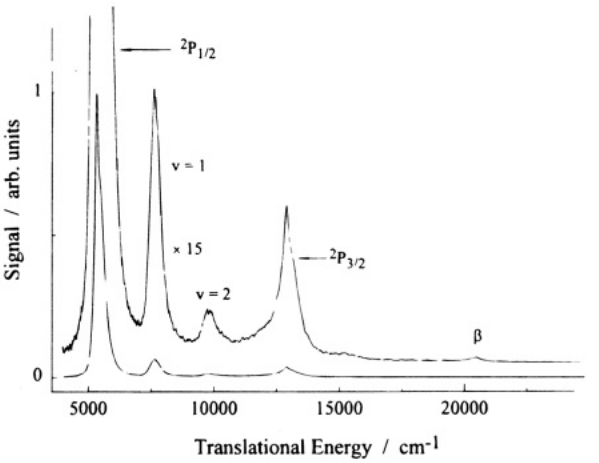

Figure 5. Translational energy spectrum taken with vertical polarization and under conditions where clusters are present (4.4% HI/Ar, ~3000 Torr, early portion of the pulsed beam). Note the peaks labeled $v = 1$, $v = 2$, and β.

III. Experimental Results

With minimal clustering and with sufficient expansion cooling to ensure that most of the HI molecules reside in the $j = 0$ level, the HRTOF spectra display two prominent peaks that correspond to the atomic iodine $^2P_{3/2}$ and $^2P_{1/2}$ spin−orbit levels. A typical result is presented in Figure 4, which also reveals a small amount of two-photon excitation that yields quite fast hydrogen atoms, i.e., 3.46 and 3.19 × 10^6 cm s^{-1}, corresponding to $E_{c.m.}$ values of 50 555 and 42 952 cm^{-1}. Note the high S/N, which can be made to exceed 10^4 for the monomer peaks under the most favorable conditions. Analogous traces are obtained with the alternate photolysis polarization (see Figure 3); however, in this case the $^2P_{3/2}$ and $^2P_{1/2}$ peak intensities are essentially reversed (*vide infra*).[24]

When a small amount of clustering is present, it can be detected by expanding the vertical scale and perusing the base line. Figure 5 shows a trace obtained with 4.4% HI in Ar at a total backing pressure of approximately 3000 Torr. Prominent peaks that are associated with clusters (i.e., those labeled $v = 1$ and $v = 2$) are present at energies that are offset from the main monomer peaks by roughly the $HI(v)$ vibrational energies. In the studies reported here, we have endeavored to work with the smallest amount of clustering that still provides adequate

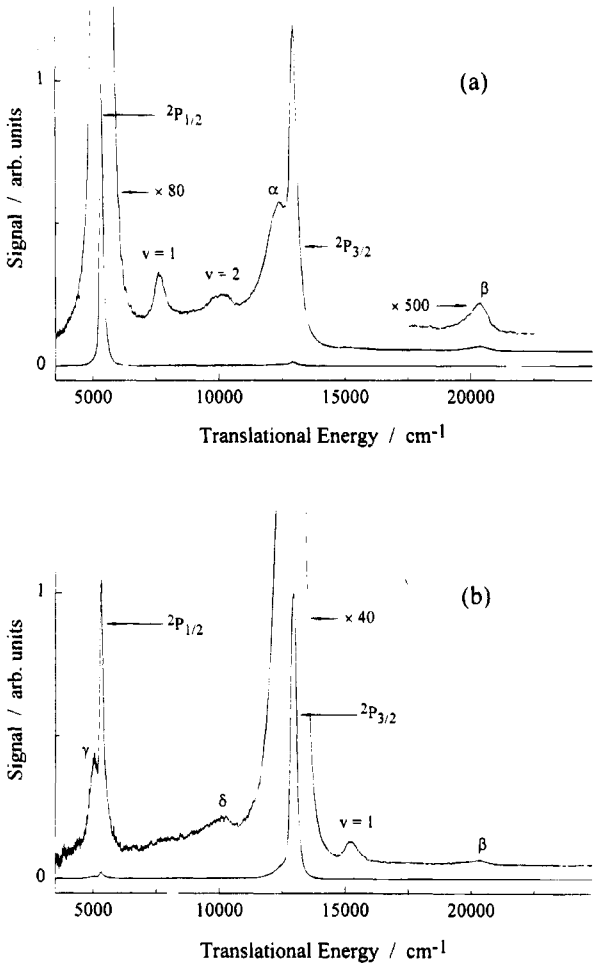

Figure 6. Translational energy spectra recorded with HI/He samples. The photolysis laser energy is 10 mJ, and there is very little clustering; (a) and (b) are for vertical and horizontal polarizations, respectively (see Figure 3). Though the full-scale traces display no obvious signs of clustering, scale expansion reveals the same structured features as shown in Figure 5.

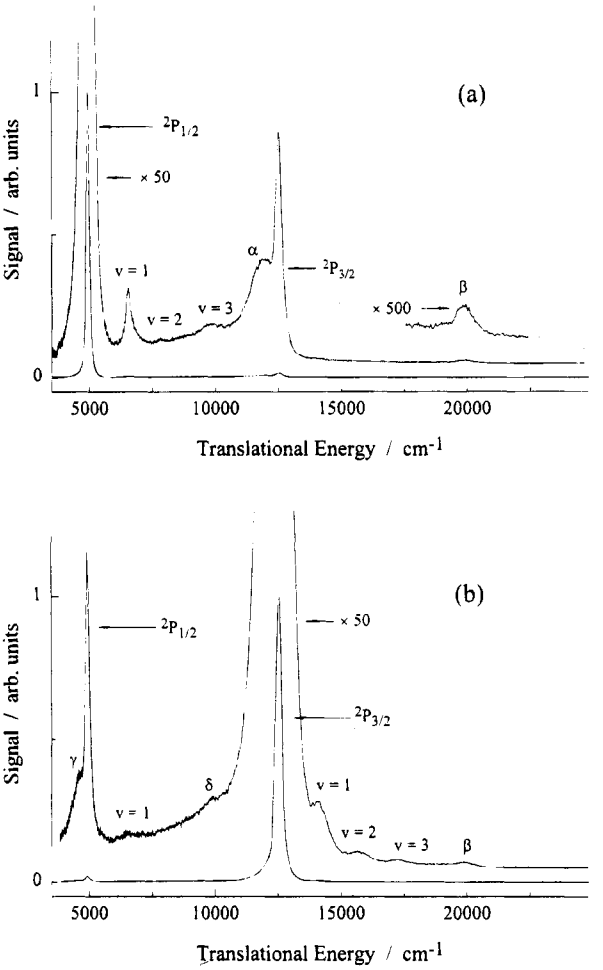

Figure 7. Translational energy spectra recorded with DI/He samples. The photolysis energy is 18 mJ, and the beam conditions are the same as for Figure 6; (a) and (b) are for vertical and horizontal polarizations, respectively.

signals in order to avoid the complications brought about by the presence of higher-than-binary clusters.

Typical translational energy spectra under conditions of very modest clustering are shown in Figures 6 and 7. By probing different parts of the expansion of HI/He mixtures, different degrees of HI clustering could be accessed. This was demonstrated by acquiring TOF spectra at different parts of the gas pulse. The areas of the $v = 1$ peak and the main monomer peak (i.e., $v = 0$) are scaled and plotted versus delay time in Figure 8. The delay time reflects the time needed for the pulsed valve to open plus the transit time for the gas pulse to reach the interaction region. It is obvious that clustering is modest in the early portion of the pulsed beam. Similar results were observed by Burnett and Young.[5b] The data shown in Figures 6 and 7 were recorded early in the expansion (4.4% HI in He at a total pressure of 1900 Torr and a delay time of about 650 μs), where clustering is known to be modest. We believe that the clusters are predominantly binary under the beam conditions for the spectra presented in Figures 6 and 7. Note that the full-scale traces in Figure 6 (i.e., those with no scale expansion) reveal only the monomer peaks, underscoring both the utility of the high S/N of the present experiments and the modest degree of clustering. As with the data shown in Figure 5, of the many distinct features, the cluster peaks labeled $v = 1$ and $v = 2$ in Figure 6 are among the most prominent. These are

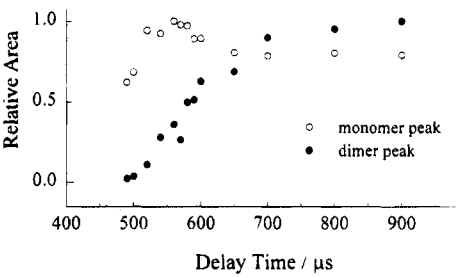

Figure 8. Areas of the $v = 1$ peak (filled circles) and the primary monomer peak (open circles) versus photolysis laser delay time for 4.4% HI in He at 1900 Torr. The maximum for each plot is rescaled to unity. The delay time is between the trigger of the pulsed valve and the firing of the photolysis laser; it reflects the valve opening time as well as the time required for the gas to reach the interaction region.

readily assigned to H atom TOF peaks from vibrationally excited HI molecules by H → D substitution, as shown in Figure 7. On the other hand, the peak labeled β, which is displaced from the high-energy monomer peak by approximately the iodine spin–orbit energy, is affected little by H → D substitution.

As shown in Figure 9, there is little if any significant difference in the $v = 1$ peak shapes obtained under the conditions of Figures 5 and 6, despite the higher probability of contributions from higher-than-binary clusters under the conditions of Figure 5, i.e., higher backing pressure and Ar carrier.

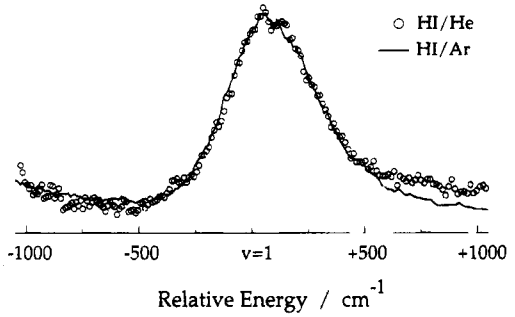

Figure 9. Comparison of $v = 1$ peaks from Figures 5 (solid line) and 6a (open circles). Though the cluster concentrations are higher under the conditions of Figure 5, there are no significant differences between the traces. The energy is given relative to the $v = 1$ peak.

This supports our assumption of negligible contributions from higher-than-binary clusters under the present experimental conditions.

Spectra recorded with different photolysis fluences (Figure 10) verified that the features labeled $v = 1$ and β are not associated with a one-photon process. Because the S/N of the $v = 2$ feature was low, its fluence dependence could not be determined. A number of such traces were recorded for photolysis energies in the range 3−10 mJ. To the best of our ability to judge, we find that the $v = 1$ and β signals vary quadratically with the photolysis fluence. Since these features are produced within the short photolysis pulse of 7 ns duration, and because the number density of the skimmed molecular beam at the interaction region (which is 7 cm from the nozzle) is low, we conclude that these features derive from binary clusters as opposed to intrabeam collisions.

To summarize, data such as those shown in Figures 5−10 indicate that a number of species and mechanisms are involved in the physical and chemical processes that occur in the unique microcosm of weakly-bound $(HI)_2$ clusters that are excited at ultraviolet wavelengths.

IV. Discussion

(a) Photolytic Removal of Atomic Hydrogen from $(HI)_2$ without Intracluster Reaction: Production of Radical−Molecule Clusters. The ultraviolet photodissociation of one of the HI moieties within $(HI)_2$ yields, among other things, weakly-bound radical−molecule clusters:

$$(HI)_2 + h\nu \rightarrow I{-}HI + H \rightarrow I^*{-}HI + H \quad (5)$$

where I−HI and I*−HI represent weakly-bound clusters that correlate at long range to I + HI and I* + HI, respectively. It is known that 266 nm photodissociation of free HI yields a significant percentage of I*, i.e., 35−40%,[8,9] and it is assumed that this remains true upon complexation of the HI moiety. Moreover, terminologies like I−HI and I*−HI are not meant to suggest anything about the geometries of the weakly-bound clusters. Considering the likely internal energies of I−HI and I*−HI brought about by their photolytic production, structure considerations may prove somewhat moot. At this point we leave open the possibility that the radical−molecule clusters indicated in eq 5 can be formed by departure of the *interior* hydrogen as well as the obvious case of the *exterior* hydrogen. Specifically, whereas three fragments will be formed to some extent by photodissociation of the HI moiety containing the interior hydrogen, the large hydrogen intermolecular zero-point amplitudes ensure that departure of the interior hydrogen will yield radical−molecule clusters a good percentage of the time.

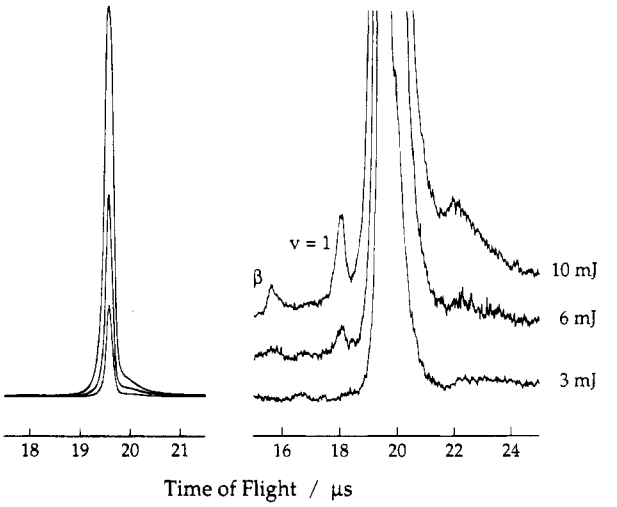

Figure 10. Fluence dependence; the right traces are expanded 100 times, horizontal polarization.

As discussed below, near-axial hydrogen trajectories are expected to give rise to inelastic scattering, which facilitates the formation of three fragments.

As shown in Figure 2 for the analogous Cl + HCl system,[16,17] there are three adiabats (right-hand column), all of whose minima lie at the linear configurations. The diabats (left-hand column) were obtained by using a coupled basis characterized by j_a and its projection on the intermolecular axis, ω. From the differences between the diabats and adiabats, it is clear that the off-diagonal terms of the potential are important. At long range, adiabat 3 correlates mostly with $j_a = {}^1/_2$, while adiabats 1 and 2 remain thorough admixtures of the $\omega = {}^1/_2$ and ${}^3/_2$ diabats of $j_a = {}^3/_2$. Hereafter, I*−HI will be used to refer to adiabat 3 while I−HI will refer to adiabats 1 and/or 2. Of the global minima, the two associated with $j_a = {}^3/_2$ have the hydrogen between the two iodine atoms, while the one associated with $j_a = {}^1/_2$ (adiabat 3) has the hydrogen on the outside. Adiabat 1 is bound by 383 cm^{-1} while adiabat 2 is bound by only 94 cm^{-1}. Adiabat 3 is bound by 133 cm^{-1} and is very isotropic in the angular coordinate with a barrier to rotation of only about 30 cm^{-1}. Thus, even modest internal (V,R) excitation on this adiabat may lead to a near-isotropic distribution of hydrogen positions. Though these characteristics were derived for the Cl + HCl system, they are expected to carry over qualitatively to the I + HI system under consideration here.

Referring to Figure 1, departure of the exterior hydrogen imparts insufficient recoil to its iodine atom to break the weak van der Waals bond. In this case, the resulting triatom has access to the linear parts of the three adiabats, i.e., where minima are located, and fragmentation of the triatom left behind is unlikely. For example, note that the nature of the binding, though it involves electronic orbitals on the halogen atom, is such that there are no low-lying repulsive curves, such as those that arise from antibonding orbitals. Moreover, because of the floppiness of $(HI)_2$, there will be a range of orientations of the electron orbitals of the $^2P_{3/2}$ atomic iodine photoproduct relative to the product triatom frame. Namely, the photolytic removal of atomic hydrogen creates a wavepacket having components that can be assigned to each of the adiabats, with I*−HI and I−HI deriving from the I* and I photoproducts, respectively.

When the hydrogen atom departs without interacting with the remaining HI, it carries away approximately 127/128 of the $E_{c.m.}$ values for reactions 1 and 2. The resulting I atom translational recoil energy is shared almost equally between overall translation and internal (V,R) excitation of the triatom

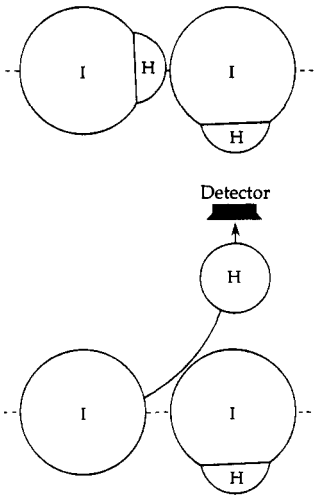

Figure 11. Schematic drawing of intracluster nonreactive scattering.

product. Thus, even for the larger of the $E_{c.m.}$ values (12 961 cm^{-1}), the triatom V,R energy is only ~50 cm^{-1}.

(b) α and γ Peaks. When the internal hydrogen atom transmits momentum to the heavier objects as per the squeezed atom effect following photoexcitation,[25] its departure can yield three fragments. This will be most efficient for near-axial trajectories, where we refer to the line between the two iodine atoms as the "axis". In general, this effect is expected to result in a low-energy tail relative to the sharp monomer peak.[3] It is noteworthy that Aker and Valentini have shown that inelastic scattering is important for HIH angles ~90°, which corresponds to near-axial trajectories in the case of $(HI)_2$ (see Figure 1), and that exchange reaction is improbable at these angles.[19]

The scattering of the interior hydrogen as it departs will impart momentum to the HI, and this may be responsible, at least in part, for the shoulders observed on the low-energy sides of the weaker monomer peaks (i.e., peaks α and γ in Figures 6 and 7). That such shoulders will appear on the low-energy sides of the weaker of the two monomer peaks is deduced from elementary considerations. Figure 11 serves as a guide. Recall that the weak monomer peaks correspond to cases in which the HI axes are aligned by photoexcitation in such a way that nearly all of the hydrogen atom fragments miss the detector in the absence of complexation. Specifically, in Figure 6, a and b, perpendicular and parallel transitions, respectively, align the HI axes such that the hydrogen atom fragments are aimed away from the detector. The weak monomer signals are due to imperfect laser polarization, the finite solid angle subtended by the detector, and molecular properties such as nonadiabatic transitions, etc. Nonetheless, the discrimination available via laser polarization is large.

With clusters, the hydrogen atoms can be deflected toward the detector, as shown in Figure 11. Thus, for signals near the weak monomer peaks, the clusters contribute in much larger proportion than their concentration relative to the monomer. Moreover, it follows that a shift is anticipated rather than just a monotonically decreasing shoulder, since the observed hydrogen atoms are deflected by ~90°. Due to momentum transfer, the downward fractional shift of the translational energy of a hydrogen atom deflected by 90° (without chattering) is given by

$$2m_H/(m_{HI} + m_H) \quad (6)$$

This corresponds to 1.55% and 3.05% for hydrogen and deuterium. For the $^2P_{3/2}$ peaks, these calculated shifts are 200 and 400 cm^{-1} for hydrogen and deuterium, respectively, while the α peaks are shifted by 560 and 620 cm^{-1} from the monomer peaks, as shown in Figures 6a and 7a. For the $^2P_{1/2}$ peaks, the estimated shifts are 80 and 160 cm^{-1}, while the γ peaks are shifted by about 260 and 340 cm^{-1} from the monomer peaks, respectively, as shown in Figures 6b and 7b. Clearly, the α and γ peaks lie at lower energies than those calculated by using eq 6. This further energy loss may be due to HI rotational excitation brought about by inelastic intracluster collisions. Note also that if the weakly-bound triatom gains sufficient internal energy via such a process, it will decompose.

To summarize, the α and γ features can be explained by simple elastic and inelastic scattering considerations. The large hydrogen zero-point amplitude yields a broad range of H → HI impact parameters, and this uncertainty, plus the experimental difficulty of measuring such scattering for alternate laser polarizations (i.e., those having the larger monomer backgrounds), lessens our enthusiasm for further pursuit of this effect under the present experimental conditions.

(c) HI Vibrational and Rotational Excitation. Next, we wish to establish to the extent possible the mechanisms responsible for the production of the $HI(v,j)$ product that derives from ultraviolet photoexcitation of weakly-bound $(HI)_2$.

First, consider intramolecular deactivation of the iodine spin–orbit excitation. The I*–HI clusters produced by reaction 5 are metastable and in the absence of photolyzing radiation will eventually decompose via internal conversion from the excited adiabat to one or both of the lower adiabats, which then dissociate on a very short (probably picosecond) time scale. This can be viewed as essentially the quenching of the atomic spin–orbit excitation which is localized on the clustered I* atom:

$$I^*–HI \rightarrow I + HI(v,j) \quad (7)$$

where the energy available for product V,R,T excitations is approximately the $^2P_{1/2}$ energy (7603 cm^{-1}) minus the energy needed to decompose I*–HI. Recall that parent I*–HI is expected to be formed with a modest amount of internal excitation. Such excitation may also facilitate reaction 7.

Since there are no near-resonant vibrational channels, electronic-to-vibrational (E–V) energy transfer is expected to be slow. It is known that the room temperature I* + HI bimolecular quenching rate constant is small (5×10^{-14} cm^3 $molecule^{-1}$ s^{-1}),[26] and it is reasonable to assume that this nonresonant process follows a positive temperature dependence.[27] Nonetheless, within the duration of the laser pulse it is conceivable that reaction 7 could yield $HI(v,j)$, which can then be photodissociated and may account in part for the $v = 1$ and $v = 2$ populations that are reflected in the translational energy spectra shown in Figures 5–7. Though $v = 0$ is also expected to be present, it is masked by the large monomer background. This will be discussed below.

Next, consider the intracluster exchange reaction of the interior hydrogen with the adjacent HI moiety. In principle, this can also contribute to the production of $HI(v,j)$:

$$IH–IH' + h\nu \rightarrow I + H–IH' \rightarrow I + HI(v,j) + H' \quad (8)$$

Finally, $HI(v,j)$ can be formed via intracluster inelastic processes involving the interior hydrogen, i.e., the cluster counterpart of gas-phase T → V,R energy transfer:

$$IH–IH' + h\nu \rightarrow I + H–IH' \rightarrow I + H + H'I(v,j) \quad (9)$$

This can be further separated into two mechanisms. In one, the photolytically produced hydrogen atom strikes the hydrogen

atom in adjacent HI; in the other, the hydrogen atom strikes the iodine part of the HI and undergoes a failed reaction.

The reactions and inelastic scattering that occur via collisions of fast hydrogen atoms with HI have been examined thoroughly under gas-phase, single-collision conditions by Aker and Valentini.[18] It was shown that the HI(v) products decrease monotonically in the ratio [v=0]:[v=1]:[v=2] = [1]:[0.10]:[0.02], while the corresponding rotational distributions extend to j = 35, 26, and 20 for v = 0, 1, and 2, respectively. In both their study and ours, atomic hydrogen was prepared by 266 nm HI photolysis, making it appropriate to compare the two sets of results, despite the different environments, i.e., gas-phase versus weakly-bound clusters. Additionally, they examined reactions of fast hydrogen atoms with HCl and HBr and have put forth a consistent picture of these H + HX (X = Cl, Br, I) systems. On the basis of the difference in rotational energy partitioning for H + HI and H + HBr as compared with H + HCl, along with the kinematics of the light + heavy−light reaction, Aker and Valentini argued that large angular momentum changes (i.e., high-j states of the HI product) are due to exchange reaction rather than inelastic energy transfer. They also point out that most (>90%) of the observed product is due to the higher of the two hydrogen speeds.

Aker and Valentini also carried out a computational study by using the method of quasiclassical trajectories.[19] A rather isotropic LEPS surface as well as a much more anisotropic DIM-3C surface, developed by Last and Baer[21] and modified by Clary,[22] were examined. They concluded that to reconcile the experimental findings it was essential to have significant angular anisotropy and that such a PES could indeed rationalize the data. On the DIM-3C surface, the minimum-energy path for the reaction is collinear with a barrier of 1020 cm^{-1}, rising to 11 270 cm^{-1} at 90°. These calculations suggested that under gas-phase conditions exchange reaction is the source of the high-j product, whereas inelastic collisions are responsible for the low-j product. Finally, an ab initio calculation of the PES was carried out by Dobbs and Dixon.[28] This surface is qualitatively similar to DIM-3C. It is noteworthy that two transition states were located: one with an HIH angle of 161° and a barrier of 1960 cm^{-1} and the other at 75° with a barrier of 5670 cm^{-1}.

The trajectory study of Aker and Valentini yielded several results that are directly relevant to the experiments reported here. First, they concluded that little exchange reaction occurs when the hydrogen attacks the iodine part of HI at HIH angles near 90°. For the exchange reaction, near-linear approaches are strongly favored over sideways approaches. Second, inelastic scattering shows a weak angular dependence, with little difference between 90° and 180°. Inelastic scattering is due mainly to the potential energy coupling that occurs when the hydrogen atom collides with the I part of the HI, as opposed to kinetic energy coupling in which the incident hydrogen atom strikes the hydrogen in HI. It is also noteworthy that the average Δj due to inelastic scattering is 4−5 for low initial j, and no obvious correlation was found between entrance channel properties and product states. The above theoretical results provide a basis for qualitative predictions concerning photoinitiated reactions in $(HI)_2$.

As shown in Figures 12 and 13, the rotational excitation of HI deriving from intracluster processes is modest. In addition to the observed v = 1 and v = 2 levels, the v = 0 level is expected to be present, though it is hard to discern because of the large monomer peak. However, the higher of the v = 0 rotational states will show up as a high-energy wing at the edge of the monomer peak. Figure 12 shows an expanded section of Figure 6a near the $^2P_{1/2}$ peak (i.e., the v = 0 region). In

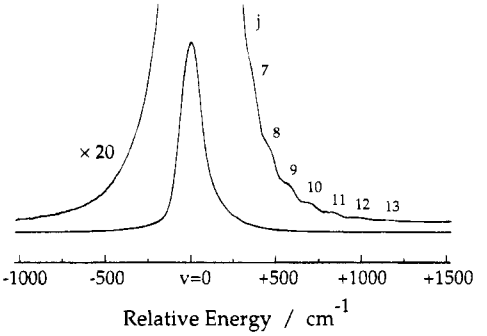

Figure 12. An expansion of the $^2P_{1/2}$ peak from Figure 6a shows barely resolved rotational structure of HI(v,j). Translational energy is given relative to the $^2P_{1/2}$ peak.

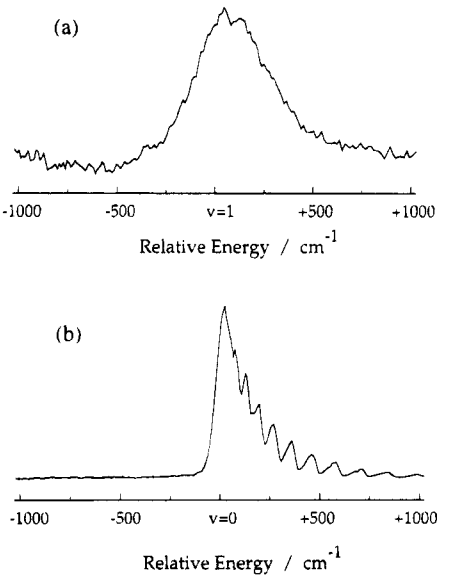

Figure 13. Comparison of (a) the v = 1 peak from Figure 6a and (b) a rotationally resolved spectrum of HI. The spectrum in (b) was obtained by lowering the backing pressure until there was little expansion cooling.

Figure 12, the barely-resolved features from 300 to 1200 cm^{-1} are assigned as rotational levels from j = 7 to j = 13. Since these features are resolved at all, the translational recoil imparted to HI(v=0) must be modest. For example, to resolve levels around j = 12 requires that the translational recoil imparted to HI(v=0) is less than ~100 cm^{-1}. This is compatible with intracluster exchange reaction and/or inelastic scattering and a modest HI recoil imparted by the squeezed atom effect. These levels would not be resolved had they derived from reaction 7, since the recoil imparted to HI(v=0) would be large, i.e., approximately half of the difference between the 7603 cm^{-1} spin−orbit energy and the triatom binding energy.

The extent of rotational excitation can also be examined near the v = 1 region (Figure 13), though the rotational levels are not resolved, possibly due to the lower S/N. Figure 13 shows a comparison between the v = 1 region and a spectrum obtained with rotationally warm HI(v=0), displaced by the vibrational quantum. The latter spectrum was obtained by lowering the backing pressure to ~50−100 Torr, where little expansion cooling occurred. It indicates that v = 1 rotational levels will be resolved in cases where the production of HI(v=1) is accompanied by minimal translational recoil imparted to this species. Note that the peak of the v = 1 feature lies close to the energy of the j = 0 level for the case of zero HI(v=1) translational recoil. Thus, the v = 1 feature can be attributed to a modest degree of rotational excitation convoluted with

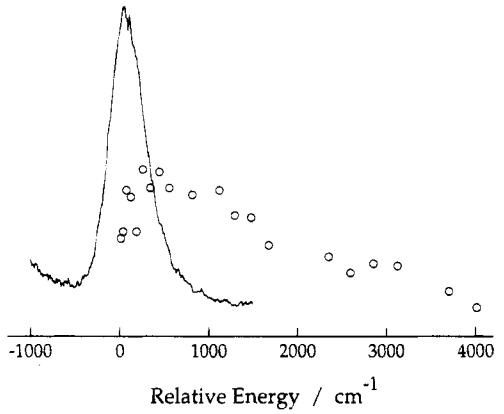

Figure 14. Comparison of the $v = 1$ peak from Figure 6a with the HI(v=1) rotational distribution determined by Aker and Valentini.[18] The spectrum denoted by circles is a direct transcription of their data; i.e., it does not take account of the Jacobian needed to convert the points to a continuous distribution.

translational motion that has been imparted to HI(v=1) during its production. A rotational distribution extending to $j \sim 12$ is compatible with the data.

Both $v = 0$ and $v = 1$ show modest rotational excitation, consistent with the results of Burnett and Young,[5b] who showed that HI(v=0) deriving from clusters contains little rotational excitation. The $v = 2$ peak also reflects modest rotational excitation, though little can be said because of the low S/N.

As mentioned above, the combination of exchange reaction and inelastic scattering has been examined under gas-phase, single-collision conditions where it was found that rotational excitation is considerable.[18] Figure 14 shows a comparison of the $v = 1$ rotational distribution taken from ref 16 and the features shown in Figure 9. Clearly, the observed features from the present experiments are considerably narrower than the energy spread associated with the gas-phase processes. It is conceivable that for the exchange reaction the constrained geometry of the precursor cluster leads to a markedly different product rotational distribution than in the case of its gas-phase counterpart. However, to our knowledge such a large difference has never been observed for any photoinitiated bimolecular reaction in a weakly-bound precursor. Furthermore, the range of hydrogen approaches associated with the weakly-bound $(HI)_2$ precursor leads to high barriers that lessen the participation of the exchange reaction channel.

The modest product HI rotational excitation observed in our experiments is consistent with the inelastic energy transfer mechanism put forth by Aker and Valentini,[19] in which low-j states are anticipated. Their trajectory studies show that inelastic energy transfer depends only weakly on the approach angle. For example, collisions with HIH angles near 90° have nearly the same energy transfer probability as at those involving collinear HIH approaches. On the other hand, the exchange reaction probability is much lower at 90°.

Gerber and co-workers examined ultraviolet photoinitiated processes in $(HCl)_2$ by using the method of classical trajectories.[3] Collisions of photolytically prepared H atoms with the adjacent HCl were examined, and it was shown that HCl products deriving from the intracluster exchange reaction are rotationally and vibrationally hotter than those deriving from inelastic scattering. This provides further support for the thesis that inelastic scattering is the more likely process in our studies.

The small peak labeled δ on the low-energy side of the monomer peak (see Figures 6b and 7b) could be due to hydrogen atoms that leave following intracluster collision; its energy loss relative to $^2P_{3/2}$ peak is roughly one HI vibrational quantum plus the shift of the α peak. The broad spread is consistent with the rotational distributions reported by Aker and Valentini, though the δ peak may correspond to both inelastic energy transfer and exchange reaction. Though the α peak is also a signature of intracluster collision, in this case HI does not gain vibrational excitation.

Now consider reaction 7. The quenching of $I(^2P_{1/2})$, as well as the quenching of other spin−orbit excited $^2P_{1/2}$ halogens,[29] has been studied extensively under gas phase conditions, though not in the environment of a weakly-bound precursor. Likewise, high-level theoretical calculations are now possible,[30] though they have yet to be applied to such systems. Since there are no near-resonant HI vibrational levels, selective HI vibrational excitation is not anticipated. Moreover, there is minimal multipolar interaction since the $^2P_{1/2}$ electric quadrupole moment is zero, as reflected in the near-isotropic angular variation shown in Figure 2 for adiabat 3.[17] Thus, I*−HI can be long-lived and may participate in further photoinitiated processes under conditions of high photolysis fluence, as discussed below.

One thing is certain: if HI(v=1) is produced via reaction 7, approximately 5000 cm^{-1} will be shared between c.m. translation and HI rotation.[31] Since product HI rotational excitation has been shown to be modest, this means that slightly less than half of the 5000 cm^{-1} will appear as HI(v=1) translation in the $(HI)_2$ c.m. system. This would broaden individual rotational levels so much that they could not be resolved at all. Moreover, the widths are expected to be even larger than the width associated with the left half of the peak shown in Figure 13a. Thus, though reaction 7 may contribute, it is probably not dominant.

The evidence presented above favors reaction 9 as the dominant, but not necessarily sole, source of vibrationally excited HI. However, since the evidence is circumstantial, this assignment is tentative. The above considerations applied to the case of $(DI)_2$ lead to the same conclusions.

(d) $H_2 + I_2$ Channel. An additional fact worth noting is that the intracluster abstraction reaction

$$(HI)_2 + h\nu \rightarrow H_2 + I_2 \qquad (10)$$

may take place, though we are blind to this channel experimentally. I_2 production from photoexcited HI clusters has been reported previously, albeit under conditions that favor the formation of large $(HI)_n$ clusters.[6] Buntine et al. observed vibrationally and rotationally excited slow H_2 molecules, in addition to the anticipated fast H_2 molecules, in their study of the photoinitiated reaction in a molecular beam.[32] The slow H_2 cannot be rationalized by a simple abstraction mechanism in the molecular beam. They speculated that the slow H_2 may derive from reaction of HI dimer or higher clusters, since their beam conditions were favorable for extensive cluster information.

Under gas-phase, single-collision conditions, the cross section for the reaction

$$H + HI \rightarrow H_2 + I \qquad (11)$$

is approximately 2 $Å^2$, consistent with the small size of the target atom.[33] For inelastic scattering the cross section is larger, about 11 $Å^2$.[18] Moreover, if the structure shown in Figure 1 is qualitatively correct, reaction 11 is discriminated against by the geometry of the cluster; therefore, it is not expected to be a dominant channel. The theoretical work of Gerber and co-workers on $(HCl)_2$ also shows that the abstraction reaction in the cluster is a minor channel (1%).[3]

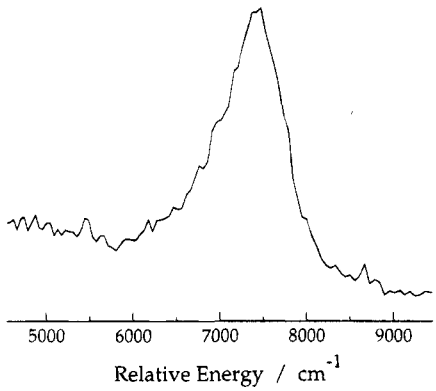

Figure 15. Expanded view of the β peak in Figure 6a. Translational energy is given relative to the $^2P_{3/2}$ peak.

Any I_2 deriving from reaction 10 will probably be formed with a large interatomic separation, i.e., characteristic of the $(HI)_2$ precursor. Moreover, iodine atoms deriving from photodissociation will be formed in both the $^2P_{3/2}$ and $^2P_{1/2}$ states. Therefore, it is likely that some of the I_2 formed via reaction 10 will be electronically excited. Experimental studies of its wavepacket dynamics could be revealing.

(e) Superelastic Scattering: The β Peak. The peaks labeled β in Figures 5−7 lie at considerably higher energies than the monomer $^2P_{3/2}$ peaks and depend only weakly on H → D substitution, shifting to slightly lower energies. Moreover, the energies of the β peaks relative to the $^2P_{3/2}$ peaks are suggestively close to the iodine spin−orbit splitting of 7603 cm^{-1}, as shown in Figure 15. One possibility is that I*−HI clusters are photoexcited in competition with reaction 7, with photoexcitation acting on the HI chromophore in I*−HI. In this case, the departing hydrogen atom can deactivate I*, for example through the involvement of known curve crossings,[12,34] thereby gaining translational energy by almost the spin−orbit splitting. Note that the high photolysis fluences used in our experiments enables photoexcitation of I*−HI clusters to compete with intramolecular spin−orbit relaxation.

This case is interesting because it involves the participation of several chemical bonds on an extremely short time scale. Though hydrogen leaves having deactivated I*, the mechanism is almost certainly more complicated than simply inelastic scattering via a repulsive I* + H curve that crosses a repulsive I + H curve.[12,34] We assume that the I−I separation is not changed much from its value(s) in the I*−HI precursor regardless of the details of the dynamics. Thus, it is formed with R_{I-I} values ~5 Å. The picture that presents itself is that species such as I*−I, I*−I*, and I−I can be formed and that the β peak is associated with I−I. There are many I_2 potential curves, repulsive as well as attractive, and this will have the effect of broadening the hydrogen translational recoil distribution. Indeed, the β peak is seen to be fairly broad, for example in comparison with the $v = 1$ peak. This β peak may someday become important grist for the mill of theory.

V. Summary

The ultraviolet photophysics and photochemistry of weakly-bound $(HI)_2$ clusters has been examined experimentally by using the high-n Rydberg time-of-flight (HRTOF) method. The main conclusions are summarized below.

1. By expanding 4−5% HI in He and probing the early part of the expansion, it is possible to maximize considerably those contributions deriving from binary clusters relative to those deriving from higher-than-binary clusters. Monomer HI of course dominates, but good TOF resolution can discriminate against the prominent monomer peaks associated with $I(^2P_{3/2})$ and $I(^2P_{1/2})$. Fluence dependence measurements enable one- and two-photon processes to be distinguished, and high fluences can be used to bring about the efficient secondary photolysis of photoproducts such as $HI(v,j)$, I−HI, and I*−HI.

2. Because of the extreme light/heavy mass combination, weakly-bound I−HI and I*−HI clusters are formed efficiently. The latter is potentially unstable due to intramolecular quenching of the atomic iodine spin−orbit excitation. Some of the departing hydrogen atoms (specifically, the *interior* hydrogens) are scattered elastically as well as inelastically from the adjacent HI during their departure, yielding a signature on the low-energy side of the monomer peak.

3. Peaks assigned to $HI(v)$ were verified by H → D substitution. For HI and DI, vibrational levels up to $v = 2$ and $v = 3$, respectively, were observed. For $HI(v=0)$, it was possible to just barely resolve rotational levels having $7 \leq j \leq 13$, indicating that the HI responsible for these features has acquired modest translational recoil, consistent with the squeezed atom effect. Rotational resolution of $v > 0$ levels was not possible, probably because of the lower S/N.

4. The most likely source of internally excited $HI(v,j)$ is inelastic scattering. This is supported by theoretical studies that employ the method of quasiclassical trajectories. Specifically, the calculations of Aker and Valentini[19] using a PES developed by Last and Baer[21] and refined by Clary[22] are particularly relevant. From these calculations it follows that the likely L-shaped geometry of $(HI)_2$ is compatible with inelastic scattering occurring with good probability via a failed reaction mechanism. However, the L-shaped geometry is unfavorable for the hydrogen exchange reaction, which prefers near-linear H−IH approaches. Additionally, the inelastic channel is expected to have average Δj values around 4−5, which is consistent with the present experimental observations as well as those of Burnett and Young.[5b] The other possible sources of internally excited HI (exchange reaction and I*−HI internal conversion), though probably not dominant, cannot be eliminated at this time.

5. Photodissociation of I*−HI can lead to hydrogen atoms having translational energies in excess of the high energy $^2P_{3/2}$ monomer peak by slightly less than the iodine spin−orbit energy. Such peaks were observed and are tentatively assigned to this process; H → D substitution resulted in only a slight downward shift, presumably due to more efficient momentum transfer. It is highly likely that some I_2 molecules are formed at large internuclear distances with a range of energies just below the bond dissociation energy.

Acknowledgment. The Department of Energy (Contract DE-FG03-85ER13363) supported all of the HRTOF development work reported herein; the National Science Foundation supported the study of the intracluster dynamics. The authors thank J. Hutson for preprints, helpful discussions, and the use of Figure 2. M. Shapiro, M. Alexander, and G. Balint-Kurti put us on the right track regarding HX photodissociation.

References and Notes

(1) Leopold, K. R.; Fraser, G. T.; Novick, S. E.; Klemperer, W. *Chem. Rev.* **1994**, *94*, 1807 and references therein.

(2) (a) Bemish, R. J.; Wu, M.; Miller, R. E. *Faraday Discuss. Chem. Soc.* **1994**, *97*, 57. (b) Bohac, E. J.; Miller, R. E. *J. Chem. Phys.* **1993**, *99*, 1537. (c) Marshall, M. D.; Bohac, E. J.; Miller, R. E. *J. Chem. Phys.* **1992**, *97*, 3307. (d) Bohac, E. J.; Marshall, M. D.; Miller, R. E. *J. Chem. Phys.* **1992**, *96*, 6681.

(3) McCoy, A. B.; Hurwitz, Y.; Gerber, R. B. *J. Phys. Chem.* **1993**, *77*, 12516.

(4) Segall, J.; Zhang, J.; Dulligan, M.; Beaudet, R. A.; Wittig, C. *Faraday Discuss. Chem. Soc.* **1994**, *97*, 195.

(5) (a) Young, M. A. *J. Phys. Chem.* **1994**, *98*, 7790. (b) Burnett, J. W.; Young, M. A. *Chem. Phys. Lett.* **1994**, *228*, 403. (c) Young, M. A. *J. Chem. Phys.*, in press.

(6) Fan, Y. B.; Randall, K. L.; Donaldson, D. J. *J. Chem. Phys.* **1993**, *98*, 4700.

(7) (a) Cho, C. C.; Polanyi, J. C.; Stanners, C. D. *J. Chem. Phys.* **1989**, *90*, 598. (b) Bourdon, E. B. D.; Cho, C. C.; Das, P.; Polanyi, J. C.; Stanners, C. D.; Xu, G. Q. *J. Chem. Phys.* **1991**, *95*, 1361.

(8) Clear, R. D.; Riley, S. J.; Wilson, K. R. *J. Chem. Phys.* **1975**, *63*, 1340.

(9) Schmiedl, R.; Dugan, H.; Meier, W.; Welge, K. H. *Z. Phys. A* **1982**, *304*, 137.

(10) Givertz, G.; Balint-Kurti, G. G. *J. Chem. Soc., Faraday Trans. 2* **1986**, *82*, 1231.

(11) Alexander, M. H.; Pouilly, B.; Duhoo, T. *J. Chem. Phys.* **1993**, *99*, 1752.

(12) Levy, I.; Shapiro, M. *J. Chem. Phys.* **1988**, *89*, 2900.

(13) Buckingham, A. D.; Fowler, P. W. *J. Mol. Struct.* **1988**, *189*, 203.

(14) Hannachi, Y.; Silvi, B. *J. Mol. Struct.* **1989**, *200*, 483.

(15) Engdahl, A.; Nelander, B. *J. Phys. Chem.* **1986**, *90*, 6118.

(16) Dubernet, M.; Hutson, J. M. *J. Chem. Phys.* **1994**, *101*, 1939.

(17) Dubernet, M.; Hutson, J. M. *J. Phys. Chem.* **1994**, *98*, 5844.

(18) Aker, P. M.; German, G. J.; Tabor, K. D.; Valentini, J. J. *J. Chem. Phys.* **1989**, *90*, 4809.

(19) Aker, P. M.; Valentini, J. J. *J. Phys. Chem.* **1993**, *97*, 2078.

(20) Segall, J.; Wen, Y.; Singer, R.; Dulligan, M.; Wittig, C. *J. Chem. Phys.* **1993**, *99*, 6600.

(21) (a) Last, I.; Baer, M. *Chem. Phys. Lett.* **1980**, *73*, 515. (b) *J. Chem. Phys.* **1981**, *75*, 288.

(22) Clary, D. C. *Chem. Phys.* **1982**, *71*, 117.

(23) Schneider, L.; Meier, W.; Welge, K. H.; Ashfold, M. N. R.; Western, C. *J. Chem. Phys.* **1990**, *92*, 7027.

(24) The peak intensities are reversed in the sense that the strong becomes weak and the weak becomes strong.

(25) Wittig, C.; Engel, Y. M.; Levine, R. D. *Chem. Phys. Lett.* **1988**, *153*, 411.

(26) (a) Donovan, R. J.; Fotakis, C.; Golde, M. F. *J. Chem. Soc., Faraday Trans. 2* **1976**, *72*, 2055. (b) Pritt, A. T.; Coombe, R. D. *J. Chem. Phys.* **1976**, *65*, 2096.

(27) Yardley, J. T. *Introduction to Molecular Energy Transfer*; Academic Press: New York, 1980.

(28) Dobbs, K. D.; Dixon, D. A. *J. Phys. Chem.* **1993**, *97*, 2085.

(29) Houston, P. L. *Adv. Chem. Phys.* **1981**, *47*, 381.

(30) Amatatsu, Y.; Yabushita, S.; Morokuma, K. *J. Chem. Phys.* **1994**, *100*, 4894.

(31) The value of ~5000 cm^{-1} is the iodine spin−orbit energy (7603 cm^{-1}) minus the HI(v=1) energy minus the energy needed to break the I*−HI bond.

(32) Buntine, M. A.; Baldwin, D. P.; Zare, R. N.; Chandler, D. W. *J. Chem. Phys.* **1991**, *94*, 4672.

(33) Aker, P. M.; Germann, G. J.; Valentini, J. J. *J. Chem. Phys.* **1989**, *90*, 4795.

(34) Nikitin, E. E. *Theory of Elementary Atomic and Molecular Processes in Gases*; Clarendon: Oxford, 1974.

JP9506189